Journal of Rock Mechanics and Geotechnical Engineering 17 (2025) 7503–7514

Contents lists available at ScienceDirect

Journal of Rock Mechanics and Geotechnical Engineering

journal homepage: www.jrmge.cn

Full Length Article

Elastic response of doleritic sill to high temperatures, Sonhat Basin, India

Chinmay Sethi [a], Bodhisatwa Hazra [a,*], Ali Soleimani [b], Mehdi Ostadhassan [b,c,**], Soumyajit Mukherjee [d], Dripta Dutta [e], Jai Krishna Pandey [a]

[a] CSIR-Central Institute of Mining and Fuel Research, Dhanbad, 826001, India
[b] State Key Laboratory of Continental Shale Oil, Northeast Petroleum University, Daqing, 163318, China
[c] Institute of Geosciences, Marine and Land Geomechanics and Geotechnics, Christian-Albrechts-Universität, Kiel, 24118, Germany
[d] Indian Institute of Technology Bombay, Powai, Mumbai, 208016, India
[e] Research Institute of Frontier Science and Technology, Okayama University of Science, Japan

ARTICLE INFO

Article history:
Received 11 September 2024
Received in revised form
28 June 2025
Accepted 14 August 2025
Available online 6 September 2025

Keywords:
Uniaxial compressive strength
Young's modulus
Microfractures

ABSTRACT

Understanding the thermo-mechanical behavior of various rock types is important in a wide range of geoscientific applications. In this study, the effects of elevated temperature treatments (250 °C–750 °C) on the elastic response (wave velocities and mechanical properties) of dolerite, retrieved from a borehole in the Sonhat Basin, India, were analyzed. The results showed that uniaxial compressive strength (UCS) increased by 15.4% at 250 °C compared to their room temperature (25 °C) counterparts due to drying effects and inherent rock strengthening, but declined steadily at higher temperatures due to heat-induced microcracking and mineral transformations. Similarly, Young's modulus of the rock samples increased up to 250 °C and then decreased sharply above 450 °C, aligning with the brittle-ductile transition temperature of 450 °C. Petrographic and electron microscopy analyses of the samples revealed the development of intergranular and intragranular fractures at temperatures above 450 °C, contributing to the observed mechanical weakening. Furthermore, ultrasonic wave velocities (P- and S-waves) exhibited significant reductions with increasing temperature, highlighting microstructural damage. These findings provide critical knowledge for designing underground geological engineering structures by identifying temperature thresholds and understanding mechanical degradation under thermal stress. The findings are particularly relevant for underground coal gasification (UCG) projects in the Sonhat Coalfield, where dolerite sills overlying coal seams may be exposed to significant heat. The identified threshold temperatures and trends in mechanical behaviour provide valuable insights for addressing structural stability challenges and mitigating environmental risks, such as surface subsidence.

1. Introduction

Most of the rock-engineering applications require mechanical testing on intact rock samples at room temperature to obtain desired properties, with the response of the specimen to the applied force. However, over the past few years, understanding the thermo-mechanical behavior of various rock types has become important in underground geological applications, i.e. hard dry rock (HDR) geothermal reservoirs, underground coal gasification, underground disposal of nuclear waste, as well as carbon and hydrogen storage (Tian et al., 2017; Gautam et al., 2018; Wang et al., 2020). Besides, tunnel fires, building fires (e.g. building stone use case), etc., can also expose rocks to high temperatures, which may reduce their strength, thereby compromising the safety and stability of the structures (Ozguven and Ozcelik, 2014).

* Corresponding author. CSIR-Central Institute of Mining and Fuel Research, Dhanbad, 826001, India.
** Corresponding author. State Key Laboratory of Continental Shale Oil, Northeast Petroleum University, Daqing, 163318, China.
E-mail addresses: bodhisatwa.hazra@gmail.com (B. Hazra), mehdi.ostadhassan@ifg.uni-kiel.de, mehdi.ostadhassan@nepu.edu.cn, mehdi.ostadhassan@gmail.com (M. Ostadhassan).

Peer review under responsibility of Institute of Rock and Soil Mechanics, Chinese Academy of Sciences.

https://doi.org/10.1016/j.jrmge.2025.08.005

This prompted several researchers to investigate the influence of elevated temperatures on the stress and elastic response of the rocks (Mahanta et al., 2020; Qin et al., 2020; Wang et al., 2020; Paul et al., 2022; Yang et al., 2023). These studies showed that with rising temperature, the strength and elastic properties generally reduce, and depending upon the rock type, this change becomes drastic, especially beyond a certain temperature where thermal coefficients of individual mineral components play a crucial role. Therefore, based on the extent of thermal expansion and thermal stresses experienced by these minerals, micro-cracks can develop, which can weaken the rock (Shao et al., 2015; Sun et al., 2015; Tian et al., 2017).

The development of micro-cracks could be inter-granular, intra-granular, or both (Wang et al., 2020). Herein, certain rock properties, such as the wave velocity and porosity, are good indicators of pre-existing cracks or defects in rocks at room temperature. Based on this, a predictive model could be developed for rock strength (Barham et al., 2020). However, high-temperature treatment either creates new cracks or widens the pre-existing ones within the rock body, and this leads to variations in porosity and ultrasonic wave velocities (Shao et al., 2015) that sometimes do not follow a particular trend, which is observed in sandstones (Zhang et al., 2016). This makes it difficult to develop predictive mechanical models similar to those at room temperature. Besides, other parameters, including the heating scheme (duration, rate of heating, and rate of cooling, etc.) may also be influential in changing the mechanical response of the rock. Overall, it is necessary to increase our knowledge of the impact of heat on the strength and elastic properties of the rocks.

Several authors have investigated the temperature-induced mechanical changes in rocks. Tian et al. (2017) found that at temperatures above 600 °C, diorite samples showed a decrease in UCS and Young's modulus attributed to the development of mineral-boundary and trans-granular cracks. Similarly, studies conducted by Shao et al. (2015) and Sun et al. (2019) found that granite samples developed significant micro-cracks above the heat treatment temperature of 600 °C. Hu et al. (2018) observed that between 500 °C and 600 °C, quartz minerals in granite samples underwent a phase transition from α-quartz to β-quartz, leading to volume expansion and micro-crack formation, which significantly reduced strength. Chen et al. (2017) related the degradation of strength in granite to the volume increase of phlogopite minerals, while Zhang et al. (2016) linked thermal effects to the loss of bound and mineral-combined water at critical temperature thresholds. The varying thermal expansion rates of minerals in crystalline rocks affect the widening or closure of these cracks (Dwivedi et al., 2008). Furthermore, most studies agree that brittle rocks transition to ductile behavior beyond a certain temperature (Xu et al., 2009; Qin et al., 2020; Wang et al., 2020), but specific data on diabase, to the best of our knowledge, remain limited. While diabase shares similarities with other crystalline rocks, systematic studies on its thermally induced mechanical behavior are limited.

This study delves into the chemo-mechanical properties of dolerite samples obtained from the Sonhat coalfield, India, after exposure to heat. Considering the potential of coal seams in the study area for UCG, the surrounding layers, including dolerite sills, will be exposed to high temperatures, altering their mechanical properties and potentially impacting the stability and efficiency of the gasification site. Such deformations, if not studied in depth, may lead to surface subsidence and significant environmental impacts. Therefore, uniaxial compression tests on the dolerite samples at elevated temperatures of 25 °C, 250 °C, 450 °C, 600 °C, and 750 °C are conducted to obtain variations in peak strength, elastic properties (Young's modulus and Poisson's ratio), density, as well as ultrasonic wave velocities. Additionally, thin sections of the heat-treated dolerite samples were studied to relate heat-induced microscopic alterations in the constituent minerals with the changes observed in the strength and elastic properties. Anticipating changes in rock strength and ensuring the structural stability of UCG sites requires a thorough knowledge of the rock behavior after temperature treatment. This knowledge would allow for the implementation of effective measures to mitigate potential instability risks.

2. Geology of the study area

The analyzed dolerite samples in this study belong to the Labji-Pusla block in the central part of the Sonhat Coalfield, from the Lower Gondwana Group. The area is primarily covered with a topsoil layer overlying the Barren Measure and Raniganj Formation, with sandstone outcrops present in certain regions of the block (Klootwijk, 1974). A significant geological feature of this area is the intrusion of a 130–150 m thick dolerite sill, which occurs within the Barakar Formation, approximately 200–250 m above its base, and is overlain by 500–550 m of Barakar strata (Jena et al., 2016). In the eastern part of the area, east of Pathargua, the sill gradually swings to a north-south orientation near Latma, while further west it strikes in an ENE-WSW direction. Notably, the intrusive body cuts across the Talchir Formation in the southeast and extends into the Barakar Formation (Klootwijk, 1974). West of Nagar, the dyke is observed intruding into the Talchirs, with the eastern contact appearing to be faulted. Fig. 1 presents a schematic depiction of the dolerite sill intrusion in the Sonhat Coalfield.

3. Material and methods

3.1. Sample collection and preparation

The dolerite core samples analyzed in this study were retrieved from a borehole drilled to a total depth of 529 m. Specifically, 10 samples were collected from a depth range of 298–313 m. The purpose of drilling this borehole was to identify the location of coal seams and to conduct a geotechnical study of the coal and dolerite sills. The rock samples were cut into plugs, and their density was measured with an average dry density value of 2.9 g/cm^3 that was obtained by dividing the weight by the volume of the samples. Dolerite samples were cut into cylindrical plugs of 47 mm in diameter, while the length was kept at ~94 mm per the American Society for Testing and Materials (ASTM) for UCS testing (ASTM D4543, 2010), and ultrasonic wave velocity measurements. Additionally, the specimens' edges were smoothed using a grinding apparatus to ensure that the surfaces were parallel and flat within the specified ranges of 0.05 mm and 0.02 mm, respectively (ASTM D4543, 2010). The dolerite specimens were subjected to drying in an oven at 105 °C for 12 h to eliminate any moisture from the samples (Mahanta et al., 2020). The dried samples were divided into five groups for UCS measurements at five different temperatures (25 °C, 250 °C, 450 °C, 600 °C, and 750 °C), where two samples were dedicated to each temperature point.

3.2. Testing methodology

3.2.1. High temperature treatment

The present study required heating the dolerite samples at temperatures of 250 °C, 450 °C, 600 °C, and 750 °C, in addition to one that was subjected to the load at room temperature. The dolerite specimens were heated using an electric furnace, with a temperature increase of 5 °C per minute until the desired temperatures were achieved. The specimens were exposed to the

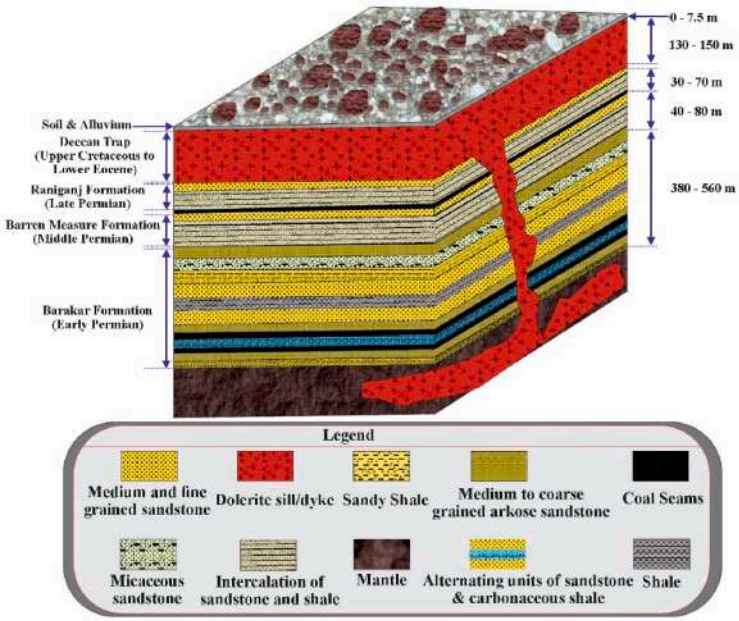

Fig. 1. Schematic depiction of the dolerite sill intrusion in the Sonhat Coalfield.

desired temperatures for 6 h to allow for uniform heat distribution throughout the samples. After the heating experiment, the high-temperature furnace was switched off to enable a gradual cooling process of the samples (Liu and Xu, 2015). Following exposure to heat, samples were transferred to a desiccator to cool down (1 h) prior to mechanical testing (Tian et al., 2017).

3.2.2. Mechanical testing procedure

A servo-controlled rock mechanics testing apparatus was employed to perform UCS tests on heat-treated samples. 2700 kN was the highest compression capacity of the equipment, and 9.0×10^9 N/m was its load frame's stiffness. A force transducer with a capacity of 1000 kN was employed to capture the data with improved resolution and accuracy. The samples were uniaxially loaded in force-controlled mode with a rate of 250 N/s until failure. The longitudinal and lateral strain of dolerite samples during compression were measured using axial (Model 632.11F-90) and circumferential (Model 632.12F-20) extensometers, respectively. Two specimens were subjected to compression tests at each temperature condition. The UCS of the dolerite samples was measured from stress values at failure, the Young's modulus was calculated from the axial stress-strain curve's linear portion, and Poisson's ratio was determined using the ratio of transverse to axial strain values at each temperature point (Chau and Wong, 1996; Malkowski and Ostrowski, 2017).

3.2.3. Measurement of wave velocities and density

Ultrasonic wave velocities (P- and S-waves) of dolerite samples were analyzed prior to the mechanical testing. In addition, density values of heat-treated dolerite plugs were measured as the ratio of mass and volume, while their P- and S-wave velocities were determined using a UlTRASONIX 4600 instrument that generates pulses and accurately measures the time of their transmissions (i.e. transit time) through the length of the specimens. The dynamic elastic properties, such as Young's modulus (E_{dynamic}) and Poisson's ratio ($\upsilon_{\text{dynamic}}$) can be estimated from the P- and S-wave velocities using the following equations (Blake et al., 2019):

$$E_{\text{dynamic}} = \rho V_S^2 \frac{3V_P^2 - 4V_S^2}{V_P^2 - V_S^2} \tag{1}$$

$$\upsilon_{\text{dynamic}} = \frac{V_P^2 - 2V_s^2}{2\left(V_P^2 - V_s^2\right)} \tag{2}$$

where V_P represents the compressional wave velocity; V_S indicates the shear wave velocity; ρ is the density of the dolerite samples; E_{dynamic} and $\upsilon_{\text{dynamic}}$ are dynamic Young's modulus and Poisson's ratio, respectively.

3.2.4. X-ray diffraction (XRD) analysis

The analysis of the mineralogical composition of the dolerite specimens, which were subjected to heat, was conducted using an X-ray diffractometer from Rigaku Corp. The XRD system employed Cu Kα radiation, which has a 1.5406 Å wavelength, and features a precise theta-theta goniometer along with a sample holder in horizontal orientation for accurate measurements. The X-ray tube was set to 40 kV (voltage) and 45 mA (current) for operation (Sharma et al., 2023). A theta/2-theta arrangement, also referred to as Bragg-Brentano focusing, combined with a D/teX configuration, was used for the measurements. The scanning process ranged from 10° to 80° in 2θ, with a step size of 0.01° and a continuous rate of 10.40182° per minute (Sharma et al., 2023). The identification of minerals was done using the ICDD PDF-2 (2018) database.

3.2.5. Microscopic analysis

Five cubic samples from the core with 10 mm × 10 mm × 10 mm dimensions were prepared at each temperature point for microscopic observations. The cubes were exposed to heat at the same experimental temperatures (25 °C, 250 °C, 450 °C, 600 °C, and 750 °C), in an electric furnace, and then each cube was carefully embedded in resin to stabilize it for cutting. Using a precision saw, the cubes were cut into flat slabs of uniform thickness, around 30 μm. The slabs were subsequently affixed to glass slides with the aid of epoxy resin as the bonding agent. The mounted slabs underwent grinding and lapping processes to achieve a smooth and

flat surface, essential for microscopy work. After achieving the desired surface quality, thin sections were polished to a high gloss using fine abrasives and polishing compounds. Finally, the prepared thin sections were thoroughly cleaned to remove any debris or residues, and a cover slip was applied using a transparent adhesive to protect the specimen and provide a clear viewing surface under the optical microscope. Additionally, the room temperature dolerite sample and its thermally treated counterparts, each measuring 0.5 mm × 0.5 mm × 0.5 mm, were gold-coated for 2 min before being examined with a field emission scanning electron microscope (FE-SEM) by Zeiss. The analysis was conducted using the Secondary Electron (SE2) scanning mode to understand the micro-crack development in the dolerite samples induced by thermal treatment.

4. Results

4.1. Petrographic analysis

Fig. 2 depicts the photomicrographs of dolerite samples subjected to heat at various temperatures. Thin section analysis of the heat-treated dolerite samples, under an optical microscope, revealed plagioclase and clinopyroxene (augite) as the dominant phases (Fig. 2a–d). The samples exhibited typical ophitic/subophitic textures: euhedral and tabular-shaped plagioclase laths are completely/partially inside the augite porphyroclasts (Fig. 2c and e). The plagioclase laths are approximately 1–1.5 mm long and do not display preferred orientation. Minor amounts of quartz were observed in the room-temperature sample, where they occupy interstitial spaces between the plagioclase laths (Fig. 2a and b). In Fig. 2c, the sample heat-treated to 250 °C shows that fractures developed in the augite grains, whereas no fractures were observed in the adjacent plagioclase grains. This indicates a differential impact of temperature treatment on the constituent minerals. With increasing temperature, the development of fractures in the mineral grains also increased. At a temperature of 450 °C, intergranular fractures were observed in both augite grains and plagioclase laths, and intragranular fractures between the augite and plagioclase laths. At even higher thermal treatment temperatures (>450 °C), the thin sections of dolerite samples revealed increased intergranular fractures within the augite grains and plagioclase laths (Fig. 2e). Similarly, increased intragranular fractures were also seen between the augite and plagioclase laths (Fig. 2f).

4.2. FE-SEM analysis

The development of micro-cracks due to the exposure to heat was examined with an electron microscope (Fig. 3). At room temperature, the dolerite samples showed no pre-existing natural cracks. Similarly, no pre-existing or micro-cracks caused by heating were found in the samples exposed to heat treatment at 250 °C (Fig. 3a and b). However, intergranular and intragranular micro-cracks induced by thermal treatment were found in the samples at 450 °C, 600 °C, and 750 °C (Fig. 3c, d, and e, respectively). In the specimens subjected to heat at 450 °C, micro-cracks with widths ranging from 0.18 μm to 0.71 μm were observed. Similarly, in the samples that were heated at 600 °C, the aperture of micro-cracks was increased, ranging from 1.08 μm to 2.16 μm, as a result of thermal treatment. Ultimately, at the highest treatment temperature of 750 °C, the crack aperture in the dolerite sample was increased further, from 0.57 μm to 4.16 μm.

Fig. 2. Photomicrographs of dolerite samples treated at different experimental temperatures. The yellow arrows point to the intergranular fractures, and the red arrows to intragranular fractures (Plag: Plagioclase; Cpx: Clinopyroxene (Augite); Qz: Quartz).

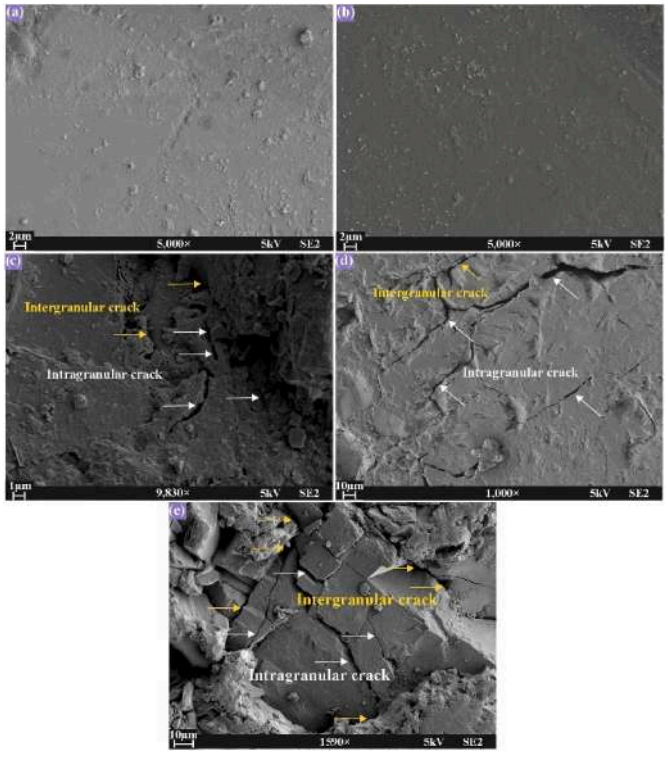

Fig. 3. Electron micrographs of dolerite samples at temperatures of (a) room temperature, (b) 250 °C, (c) 450 °C, (d) 600 °C, and (e) 750 °C. Arrows indicate the development of heat-induced intergranular and intragranular cracks.

4.3. XRD analysis

Table 1 summarizes the mineralogical composition of dolerite samples exposed to elevated temperatures. The samples mainly consist of feldspar minerals (albite and orthoclase), pyroxene (augite), and quartz. Notably, there was no alteration in the mineralogical composition after exposure to elevated temperatures. The composition of the major minerals remained stable across all heating conditions, with albite ranging from 38.4 wt% to 38.54 wt%, orthoclase from 39.1 wt% to 39.7 wt%, augite from 20.79 wt% to 20.89 wt%, and quartz from 1.48 wt% to 1.49 wt% (Table 1). Fig. 4 illustrates the mineralogical spectrum of dolerite samples at various temperatures (Fig. 4a–f), showing no significant changes due to heating. The spectrum remained consistent across all experimental temperature ranges.

4.4. Ultrasonic wave velocities and density

The ultrasonic wave velocities (P-wave, V_P, and S-wave, V_S) of dolerite samples showed a clear temperature dependence (Fig. 5), while the density remained relatively constant. Across the temperature range, the density of the samples slightly varied, between 2924 kg/m^3 and 2978 kg/m^3, indicating minimal volumetric expansion or mass loss due to thermal treatment (Table 2). At room temperature, average V_P and V_S for room temperature samples (RT-A and RT-B) were observed to be 6.1 km/s and 2.85 km/s, respectively. After heating to 250 °C, both V_P and V_S decreased by 6.1% and 18.8%, respectively, compared to their room temperature counterparts. These reductions suggest that shear wave propagation (V_S) is more sensitive to the early development of microcracks compared to compressional wave propagation (V_P). At 450 °C, the

Table 1
Mineralogical composition of dolerite samples at different temperatures.

Temperature (°C)	Albite (wt%)	Quartz (wt%)	Orthoclase (wt%)	Augite (wt%)
25	38.4	1.48	39.33	20.79
250	38.48	1.49	39.15	20.89
450	38.54	1.48	39.1	20.87
600	38.53	1.49	39.18	20.81
750	38.36	1.48	39.37	20.79

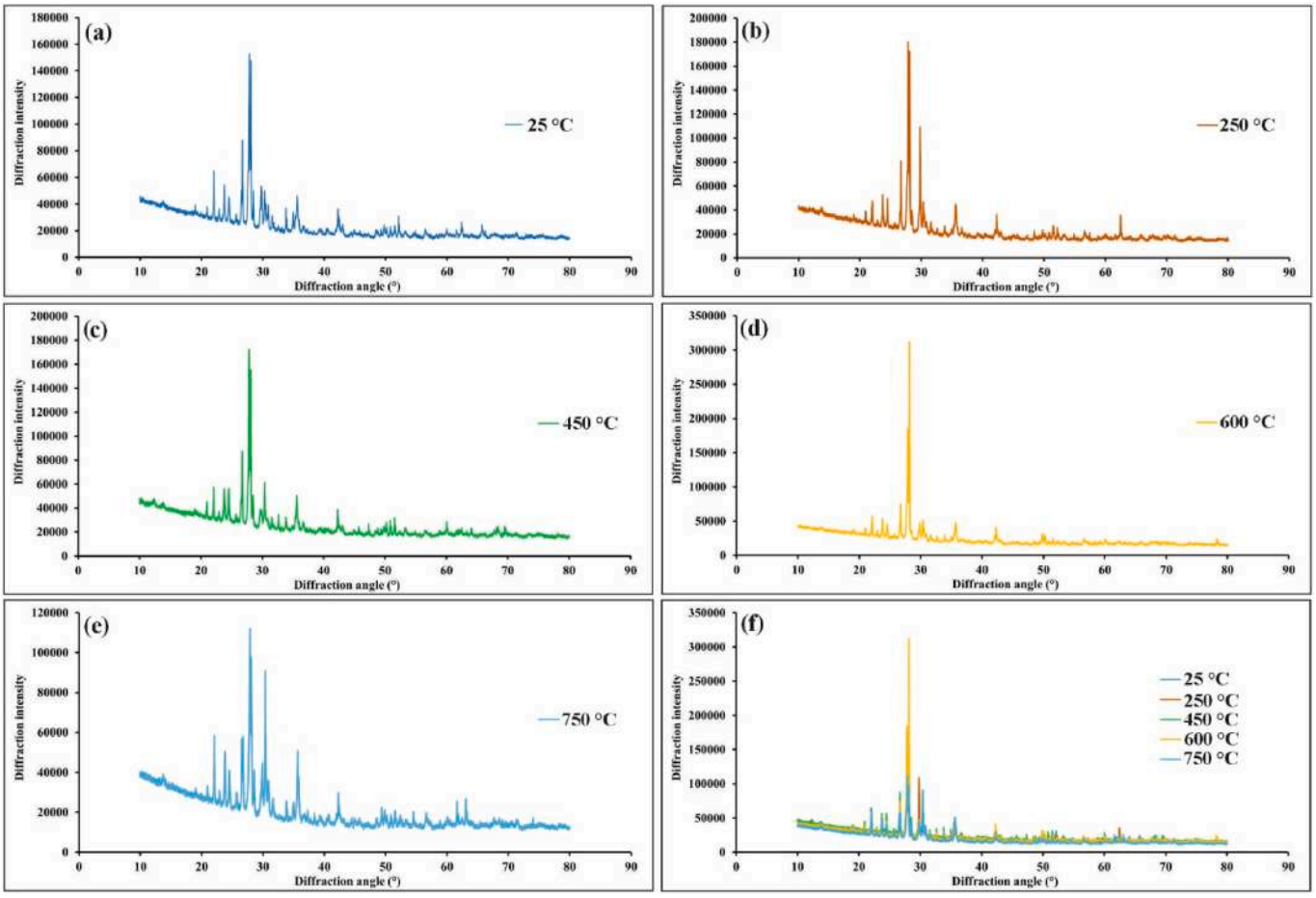

Fig. 4. Mineralogical composition and XRD spectrum of dolerite samples at room temperature (a) and after heat treatment (b–e), along with a merged spectrum showing all test temperatures (f) (RT: room temperature).

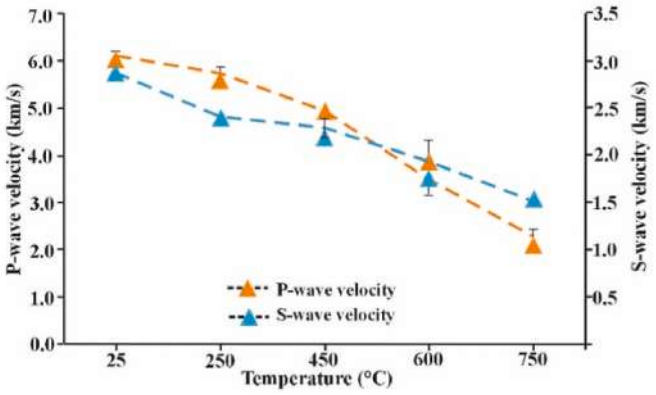

Fig. 5. A graphical presentation of the variation of V_P and V_S with increasing temperature.

reductions became more pronounced. Considering V_P, the reduction was 24.5%, while V_S decreased by 29.5%. Beyond 450 °C, the reduction in V_P became more significant relative to V_S. At 600 °C, V_P and V_S of the dolerite samples decreased by 76.8% and 46.2%, respectively. This trend underscores the growing influence of intergranular and intragranular microcracks on wave propagation with increasing temperature. At 750 °C, both V_P and V_S exhibited significant reductions, with V_P decreasing by a factor of 1.7 and V_S dropping by 90% compared to their room temperature values.

4.5. Strength and elastic properties

4.5.1. Uniaxial compressive strength

The UCS of dolerite samples exhibited two distinct trends with increasing temperature: an initial increase up to 250 °C, followed by a progressive decline at temperatures above 250 °C (Fig. 9). At room temperature, the average UCS of the dolerite specimens was observed to be 165 MPa (Table 3). At heat treatment temperatures of 250 °C, the UCS increased to 195 MPa, indicating a substantial increase in strength of up to 15.4% compared to room temperature samples. However, further increase in the heat-treatment temperature led to a reduction in UCS. At 450 °C, the UCS was 185.5 MPa, reflecting a small decline compared to 250 °C-heated samples but higher than room temperature samples. The UCS continued to decrease at temperatures above 450 °C, dropping to 122 MPa at 750 °C, marking a notable decrease of up to 35% compared to room temperature. This reduction was consistent with the development of heat-induced microcracks and mineral transformation observed in the samples with increasing heat-treatment temperatures. The failure modes of the dolerite samples also evolved with temperature. At temperatures up to 250 °C, axial splitting dominated the failure mechanism (Fig. 6c). With increasing temperature from 450 °C to 600 °C, multiple fractures developed, indicating more complex failure patterns (Fig. 6b). At 750 °C, a combination of axial splitting and shear fractures was observed, suggesting significant thermal weakening (Fig. 6c).

4.5.2. Stress-strain analysis

The stress *versus* axial and lateral strain curves were plotted for the dolerite samples subjected to varying temperature conditions (Fig. 7a and b). Based on the stress-strain curves' morphology, samples can be differentiated based on their response to the load. Essentially, axial strain and radial strains can represent rock deformation before the peak stress (Liu and Xu, 2015; Vagnon et al., 2019). It can be observed that in the dolerite samples tested at room temperature (RT-A, RT-B) and the dolerite samples heat-treated to 250 °C (250-A, 250-B), the samples have undergone failure right after reaching the peak stress (Fig. 7a). On the contrary, the dolerite samples heat-treated to temperatures of 450 °C, 600 °C, and 750 °C, deformation in the plastic region was sustained before total failure of the samples (Fig. 7b). This suggests that dolerite undergoes brittle failure at temperature below

Table 2
Ultrasonic wave velocity and density measurements of dolerite samples at various temperatures.

Temperature (°C)	Specimen No.	V_P (km/s)	Avg. V_P (km/s)	Std. dev.	V_S (km/s)	Avg. V_S (km/s)	Std. dev.	Density (kg/m^3)	Avg. density (kg/m^3)	Std. dev.
25	RT-A	6.2	6.1	0.1	2.9	2.85	0.05	2968	2939	29
	RT-B	6			2.8			2910		
250	250-A	5.9	5.75	0.15	2.4	2.4	0	2989	2978	2
	250-B	5.6			2.4			2985		
450	450-A	4.9	4.9	0	2.2	2.3	0	2871	2924	52.5
	450-B	4.9			2.4			2976		
600	600-A	3.1	3.45	0.35	1.8	1.95	0.15	2958	2950	8
	600-B	3.8			2.1			2942		
750	750-A	2.4	2.25	0.15	1.5	1.5	0	2928	2974	18.5
	750-B	2.1			1.5			2965		

Note: Avg. is short for average; Std. dev. is short for standard deviation.

Table 3
Compressive strength and static elastic properties of dolerite samples at different temperatures.

Depth (m)	Temperature (°C)	Specimen No.	UCS (MPa)	Avg. UCS (MPa)	Std. dev.	E_{static} (GPa)	Avg. E_{static} (GPa)	Std. dev.
298	25	RT-A	162	165	3	24.9	25.6	0.7
		RT-B	168			26.3		
301	250	250-A	192	195	3	27.1	26.3	0.8
		250-B	198			25.5		
305	450	450-A	186	185	0.5	25.0	24.7	0.3
		450-B	185			24.4		
307	600	600-A	152	158	6	19.8	20.8	1
		600-B	164			21.8		
313	750	750-A	124	122	2	16.5	15.9	0.6
		750-B	120			15.3		

Note: Avg. is short for average; Std. dev. is short for standard deviation.

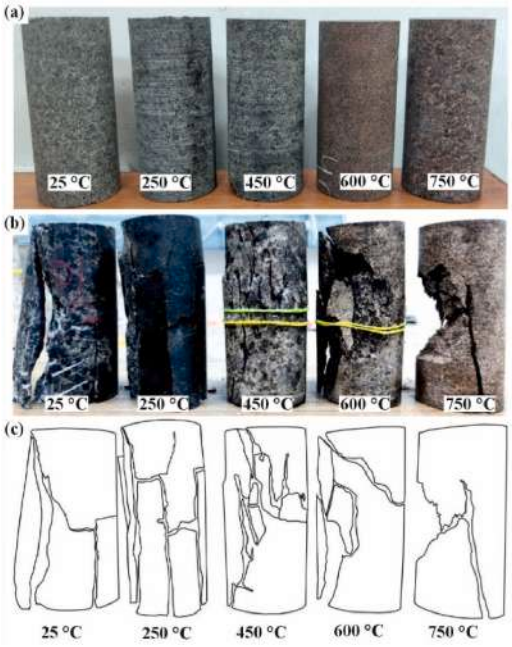

Fig. 6. Representative images of heat-treated intact rock specimens (a), deformed specimens after uniaxial compression (b), and outlines of their failure patterns (c).

450 °C. However, once the temperature surpasses 450 °C, the ductility in dolerite will improve to dominate the deformation to prevail following the peak stress, in comparison to samples at lower temperatures. To corroborate the qualitative observations from the stress-strain curves, a quantitative assessment of rock brittleness was carried out. The brittleness index was measured as the ratio of peak stress to peak strain, which reflects the resistance of the rock to deformation. A higher BI denotes a more brittle response, whereas a ductile response is indicated by lower values. The BI of the dolerite samples was normalized to facilitate the comparison across the temperature range. It was observed that the normalized BI exhibits a slight increase in brittleness up to the temperature of 250 °C, followed by a gradual decrease from 450 °C to the highest test-temperature of 750 °C (Fig. 8). The pronounced drop in brittle response of between 250 °C and 450 °C is consistent with the transition from abrupt post-peak failure in low-temperature samples to sustained plastic deformation observed in the high-temperature treated samples (Figs. 7 and 8).

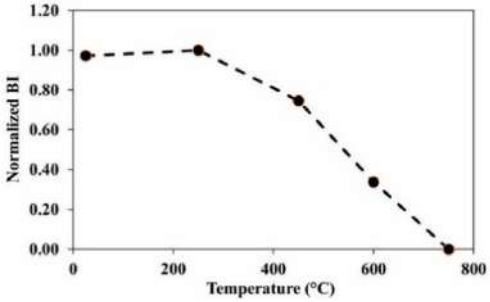

Fig. 8. Variation of the normalized brittleness index (BI) with temperature.

The crack propagation thresholds, crack closure, crack initiation, and crack damage were also identified using the stress-strain curves. The crack closure threshold was identified from the stress-strain curve as the point of transition from nonlinear to linear behaviour during the initial loading phase. The crack initiation threshold, marking the onset of new microcrack formation, was derived by detecting the deviation from linearity in the stress-strain curve beyond the crack closure region. This point is often associated with an inflection in the volumetric strain curve, where dilation begins to dominate. The crack damage threshold, representing the stress level at which existing cracks coalesce and propagate to form macro-scale fractures, was identified near the peak stress, which corresponds to the UCS. This threshold was marked by a significant deviation from linear behaviour in the post-peak region, where strain-softening and macrocrack development become prominent. It was observed that for the studied dolerite samples, with increasing temperature, crack initiation and damage occur at reduced stress levels, while the range of stable crack propagation widens (Fig. 9).

4.5.3. Static and dynamic elastic properties

The elastic properties of dolerite, static Young's modulus (E_{static}) and dynamic Young's modulus ($E_{dynamic}$), showed distinct trends with increasing temperature (Fig. 10b). At room temperature, the average E_{static} of the dolerite sample was observed to be 25.6 GPa, while $E_{dynamic}$ was notably higher at 64.5 GPa (Tables 3

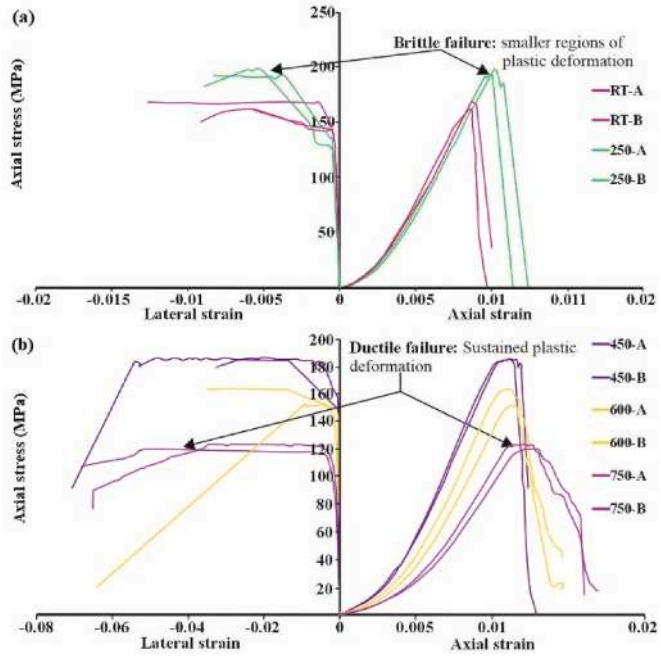

Fig. 7. Stress versus strain curves of dolerite samples showing brittle failure (a) and ductile failure (b) after heating at different temperature points.

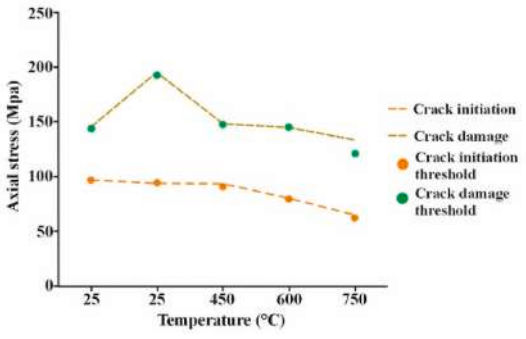

Fig. 9. Stress thresholds for crack initiation and damage, along with peak compressive strength, were measured across varying temperature conditions.

and 4, respectively). Upon heating to 250 °C, E_{static} increased to 26.3 GPa, reflecting a small enhancement of 2.7%. Conversely, $E_{dynamic}$ decreased significantly to 47.8%, showing a reduction of over 34.9% compared to room-temperature counterparts. For samples treated at 450 °C, E_{static} exhibited only a slight reduction, with a value of 24.7 GPa, whereas $E_{dynamic}$ showed a significant decline, decreasing by over 54%. This divergence highlights the increasing impact of heat-induced microcracks on dynamic wave propagation compared to static deformation. At higher treatment temperatures, both E_{static} and $E_{dynamic}$ exhibited a consistent declining trend. For samples treated at 650 °C, E_{static} decreased to 20.8 GPa, reflecting reductions up to 23.1% compared to room temperature. $E_{dynamic,}$ however, dropped more drastically to 28.8 GPa, a reduction of over 1.2 times. At 750 °C, E_{static} reduced further to 15.9 GPa, while $E_{dynamic}$ reached its lowest levels, representing a reduction of up to 3.4 times compared to room temperature.

4.5.4. Static versus dynamic Poisson's ratio

The static (υ_{static}) and dynamic Poisson's ratio ($\upsilon_{dynamic}$) of dolerite showed distinct and temperature-dependent trends, reflecting the impact of heat-induced microstructural changes (Fig. 10c). At room temperature, average υ_{static} was observed to be 0.08, while $\upsilon_{dynamic}$ was 0.36. At 250 °C heat-treatment temperatures, υ_{static} and $\upsilon_{dynamic}$ increased slightly. This increase indicates an initial adjustment in the rock's deformation characteristics due to minor thermal effects, such as drying and initial crack development. At 450 °C, both υ_{static} and $\upsilon_{dynamic}$ showed a decreasing trend, suggesting the onset of significant microcrack formation and widening within the dolerite structure. Beyond the heat-treatment temperatures of 450 °C, a divergence in trends became apparent. While υ_{static} began to increase again, reaching higher values at 750 °C, υ_{static} continued to decrease steadily. This divergence is attributed to the high-frequency ultrasonic waves used to determine $\upsilon_{dynamic}$, which are more sensitive to microcracks that disrupt wave propagation. In contrast, υ_{static} reflects the rock's deformation under low strain rates, where crack closure during static loading can lead to higher apparent values.

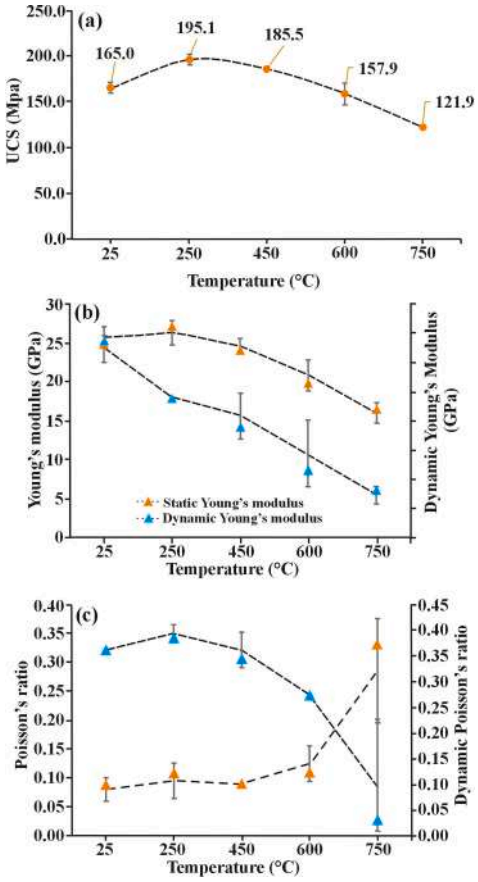

Fig. 10. Compressive strength and elastic properties of dolerite samples with increasing temperature: (A) UCS with increasing temperature; (B) static (E_{static}) and dynamic ($E_{dynamic}$) Young's modulus with increasing temperature; and (C) static (υ_{static}) and dynamic ($\upsilon_{dynamic}$) Poisson's ratio with rising temperature.

5. Discussion

This study provided critical insights into the thermo-mechanical response of dolerite exposed to high temperatures. The density of the dolerite samples exhibited minimal variation across the temperature range, remaining approximately 3 g/cm^3, even at the highest tested temperature of 750 °C. This stability can be attributed to the absence of significant material loss or volumetric expansion during heating. However, ultrasonic wave velocities, particularly the compressional wave velocity (V_P), decreased significantly with rising temperature. This trend can be explained by the progressive development of microcracks within the dolerite matrix, as observed in petrographic and SEM inspections (Section 4.2). The creation of intergranular and intragranular cracks interrupts the propagation of V_P, which is highly sensitive to the continuity of the solid and pore network. In contrast, the shear wave velocity (V_S) is less affected, as it depends primarily on the solid phase of the rock (Watanabe et al., 2024).

The UCS of the dolerite samples showed a two-stage variation. Initially, there was an increase of 19%–22% at 250 °C compared to that of the room temperature (Stage I). However, beyond 250 °C, the UCS progressively declined from 450 °C up to the highest temperature of 750 °C (Stage II) (Fig. 8). It has been reported that the UCS of the rocks may increase below a threshold temperature (T_t) and then it may decrease (Evans et al., 1990; Tian et al., 2016). The strengthening effect at stage I (<250 °C) (Fig. 8) could be attributed to the relative dominance of the 'drying' mechanism, where different minerals that are present in the samples did not undergo a major transformation, which was confirmed in micrographs (Fig. 2b and 3b, respectively). Conversely, the heat-induced damage to the dolerite mineral grains caused an overall decrease in the strength at the stage II (450 °C–750 °C) (Fig. 8). Intragranular fractures were observed in the augite grains at treatment temperatures below 450 °C (Fig. 2d). Intergranular fractures between the augite grains and plagioclase laths have also started to develop from 450 °C up to 750 °C (Fig. 2d). The propagation of cracks in igneous rocks is influenced both by fracturing at the boundaries of the grain and by inter-granular fractures within the mineral components that are weak, such as feldspar grains (Brace et al., 1972; Shao et al., 2015). Since feldspar minerals are the dominant component of the studied dolerite samples (Table 1), they appear to have a major influence on the heat-induced reduction of the strength of the samples by exacerbating fracturing in the specimens. Similar findings have been reported for igneous rocks that are primarily composed of feldspar (Shao et al., 2015; Chen et al., 2017; Huang et al., 2017). The formation of intergranular fractures between feldspar and other mineral phases (such as augite) played a critical role in reducing the load-bearing framework of the dolerite. Although quartz is present in minor quantities within the studied dolerite samples (Table 1), its contribution to microcrack initiation cannot be entirely dismissed. This could be attributed to quartz undergoing a volume expansion four times greater than that of the feldspar at elevated temperatures, leading

Table 4
Dynamic elastic properties of dolerite samples at different temperatures.

Temperature (°C)	Specimen No.	$E_{dynamic}$ (GPa)	Avg. $E_{dynamic}$ (GPa)	Std. dev.	υ_{static}	Avg. υ_{static}	Std. dev.	$\upsilon_{dynamic}$	Avg. $\upsilon_{dynamic}$	Std. dev.
25	RT-A	66.8	64.5	2.3	0.07	0.08	0.01	0.36	0.36	0
	RT-B	62.2			0.09			0.36		
250	250-A	47.5	47.8	0.3	0.08	0.1	0.02	0.4	0.39	0.01
	250-B	48.1			0.11			0.38		
450	450-A	37.7	41.7	4	0.09	0.09	0	0.38	0.36	0.02
	450-B	45.7			0.09			0.34		
600	600-A	23.1	28.8	5.65	0.14	0.13	0.02	0.27	0.27	0
	600-B	34.4			0.11			0.27		
750	750-A	16.1	14.6	1.5	0.24	0.29	0.04	0.16	0.10	0.07
	750-B	13.1			0.33			0.03		

Note: Avg. is short for average; Std. dev. is short for standard deviation.

to fracture initiation (Mahanta et al., 2020). At 573 °C, quartz transitions from α to β phase, leading to an expansion in the volume of the mineral particles, thereby introducing internal stress that eventually alters rock mechanical properties and response of the specimens to external stresses (Ringdalen, 2015; Sirdesai et al., 2017; Zhu et al., 2021). However, due to its limited abundance in the studied samples, the quartz phase transition alone cannot be considered the dominant factor in the brittle-ductile transition. Instead, the combined effects of thermal expansion mismatches and microcrack propagation in feldspar-augite networks are likely the primary drivers of the mechanical weakening observed. Several studies have found 400 °C–600 °C as the T_t for igneous rocks and have justified that by the phase change in quartz (Sun et al., 2015; Zhang et al., 2018; Qin et al., 2020; Wang et al., 2020; Li et al., 2022).

As the temperature rose, the shift from brittle to ductile behavior in the examined dolerite sample represented the two-phase change noted in the UCS of the specimens. The stress-strain curves of stage I exhibited brittle deformation, whereas in stage II, dolerite samples underwent ductile deformation (Fig. 7a and b), implying a critical change in the deformation behavior after thermal exposure. The temperature at which the studied dolerite samples transitioned from brittle to ductile was found to be 450 °C. This transition can be attributed to the combined effects of thermal expansion, phase transformations, and microstructural changes within the dolerite. The differential thermal expansion rates among feldspar, augite, and quartz resulted in stress accumulation and promoted fracture initiation, particularly at feldspar-rich grain boundaries and interfaces. Additionally, the ductile deformation beyond 450 °C is associated with the relaxation of elastic strains through microcrack coalescence and the opening of grain boundaries. These processes reduce the effective load-bearing capacity of the dolerite, facilitating sustained deformation in the plastic region of the stress-strain curve (Yin et al., 2016). Furthermore, the observed reduction in dynamic wave velocities correlates with these structural changes, as fracture density and aperture would increase with temperature, impairing wave propagation. As a result, the elastic modulus diminishes and strain increases with elevated temperatures. For the studied dolerite samples, E_{static} corresponds with the observed brittle-ductile transition phenomenon. The E_{static} increased up to 250 °C and then gradually decreased between 450 °C and 750 °C (Fig. 10b). This pattern conforms with the heat-induced intergranular and intragranular fractures development between 450 °C and 750 °C, as revealed by petrographic observations (Fig. 2c–f) as well as electron micrographs (Fig. 3c–e). The formation and subsequent increase in the aperture of intergranular and intragranular fractures with temperature in this range resulted in further ductility of the specimens (Fig. 3c–e). In contrast, the $E_{dynamic}$ showed a decreasing trend starting from 250 °C, as a result of slower ultrasonic wave propagation velocities (Fig. 10b). Optical microscopy revealed the presence of microfractures in augite (Fig. 2c), which have likely impacted the V_P and V_S that are input in $E_{dynamic}$ calculations. Overall, a significant correlation was found between the E_{static} and $E_{dynamic}$ values for the dolerite samples (Fig. 10b). It was also noted that the E_{static} values were smaller than the $E_{dynamic}$ (Tables 3 and 4, respectively) as it was generally expected (Kang et al., 2010; Shojaei et al., 2014; Yin et al., 2023). The dominance of feldspar and the associated thermally induced fractures in the dolerite samples accounts for this difference which was detected via slower wave propagation velocities with temperature as well as microscopic observations. In contrast, the υ_{static} of the dolerite samples did not exhibit consistent change with increasing temperatures (Fig. 10C).

For a better understanding of the impact of thermal treatment on the development of microcracks and their influence on elastic properties, a simplified crack density parameter (η) was obtained using the reduction in V_P relative to the measured velocity of the untreated sample as follows:

$$\eta = \frac{V_{P0} - V_P}{V_{P0}} \tag{3}$$

where V_{P0} is the P-wave velocity of the untreated sample, and V_P is the P-wave velocity after thermal treatment. This index serves as a first-order approximation to compare the extent of thermal cracking across different samples. It should be noted that this is not a comprehensive micromechanical crack density estimate, as it would require detailed information on crack geometry, orientation, aspect ratio, and anisotropy in wave velocities. However, this first-order approach shows a relative index of crack-induced degradation of velocity, which can be correlated with the changes in mechanical properties.

Table 5 shows the calculated η values, which increased from 0 at 25 °C to 0.63 at 750 °C, consistent with progressive thermal damage and microcrack accumulation. Furthermore, to assess the sensitivity of elastic properties to crack density, the ratio of static to dynamic Young's modulus was compared at different test temperatures. A consistent increase in the ratio of $E_{static}/E_{dynamic}$ was observed with an increase in the estimated crack density (η) (Fig. 11), indicating that the disparity between the two moduli decreases as thermal cracking becomes more prevalent. At lower temperatures, the dynamic modulus measured from high-frequency elastic wave propagation primarily reflects the

Table 5
Estimated simplified crack density with increasing temperature.

Temperature (°C)	25	250	450	600	750
Simplified crack density, η	0	0.06	0.2	0.43	0.63

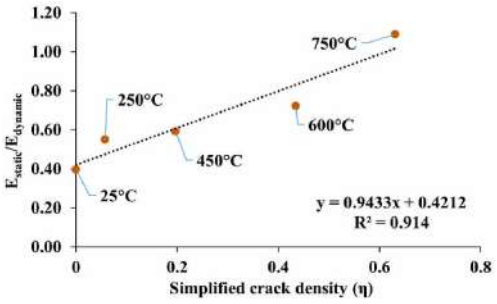

Fig. 11. $E_{static}/E_{dynamic}$ versus simplified crack density (η) with increasing temperature.

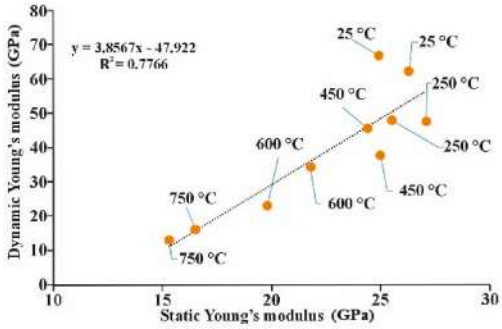

Fig. 12. Correlation between the static Young's modulus (E_{static}) and dynamic Young's modulus ($E_{dynamic}$) of dolerite samples.

properties of the intact mineral framework and is less sensitive to small-scale microcracks. On the other hand, the static modulus, measured under slow mechanical loading, is possibly more immediately affected by the presence of microcracks, particularly those influencing deformation at the grain boundaries. However, with the increase in heat-treated temperature, the microcrack network expands in density and connectivity, which results in the dynamic modulus also becoming increasingly influenced by crack-induced degradation of stiffness. This results in a relatively larger reduction in $E_{dynamic}$, thereby causing a reduction in the gap between E_{static} and $E_{dynamic}$.

In general, the brittle-ductile transition temperature of 450 °C in this study aligns well with the observed variations in the samples' strength and elastic moduli. Table 6 summarizes the temperature thresholds (T_t) beyond which a decrease in compressive strength and elastic nature of hard crystalline rocks has been observed in various studies. The T_t for granite varies due to differences in mineral composition and microstructural properties of granites from different locations (Shao et al., 2015). This necessitates assessment of the strength and elastic properties of the targeted host rock before commencing underground geological engineering projects involving high-temperature operations. Additionally, Fig. 12 highlights the relationship between the static and dynamic modulus across the temperature range where a strong correlation is seen, whereby static modulus can be estimated from dynamic values with good accuracy.

Findings of this study can provide valuable insights for designing and constructing underground geological engineering systems, specifically in the context of UCG, where the strength and elastic characteristics of the samples can change as they are exposed to higher temperatures. The dolerite sills in the study area, which overlie coal seams, will be subjected to significant heat if the coal seams are considered for gasification through the UCG process. We understood that heat can affect the mechanical behaviour of the dolerite with a substantial reduction in strength and elastic modulus beyond 450 °C, which could affect the overall stability of the gasification site. The heat-induced fracturing and brittle-to-ductile transition of the dolerite must be carefully considered in modelling efforts to ensure its structural integrity during and following the gasification process. The observed reduction in ultrasonic wave velocities and the development of thermally induced microcracks further highlight the potential for structural degradation over time. Overall, the temperature threshold of the studied dolerite samples offers a critical reference for engineers to anticipate potential changes in rock strength and elastic properties to implement necessary measures to safeguard structural stability of the gasification site and mitigate environmental impacts of such operations, particularly the collapse of the UCG chamber and surface subsidence, which has been reported in various studies (Laouafa et al., 2016; Jiang et al., 2024). However, it should be noted that the present study was conducted on a limited number of core samples at laboratory scale under uniaxial loading and dry heating conditions. Therefore, these controlled conditions may not fully capture the complex thermo-hydro-mechanical and stress environments encountered in actual underground rock masses. As such, while the findings offer a valuable reference, their direct applicability to UCG operations at the field scale should be made with caution. Future investigations would include large sample sets and confining pressure conditions to understand the impact of subsurface conditions on the thermo-mechanical behaviour of dolerite.

Table 6
Summary of the thermally-induced mechanical changes observed in hard rocks from the literature.

Sampling location	Rock type	Start in decreasing trend of UCS (°C)	Maximum temperature (°C)	Brittle-ductile transition temperature (°C)	Source
Shandong, China	Granite	>500	800	400–600	Sun et al. (2015)
Northeastern Victoria, Australia	Strathbogie Granite	>200	1100	600–800	Shao et al. (2015)
China	Granite	>25	800	600	Yin et al. (2016)
Nan'an City, China	Granite	>200	1000	800	Chen et al. (2017)
Fujian Province, China	Granite	>150	900	600	Huang et al. (2017)
Beijing, China	Diorite	>400	1000	600	Tian et al. (2017)
Rajasthan, India	Granite	>300	600	600	Gautam et al. (2018)
Dabie Mountains, China	Granite	>500	900	–	Zhang et al. (2018)
Fangshan District, China	Granite	>600	1000	600	Qin et al. (2020)
Eibenstock, Germany	Granite	>600	1000	–	Wang et al. (2020)
Hunan Province, China	Granite	>300	700	600	Zhang et al. (2022)
Sichuan Province, China	Granite	–	1000	500–550	Jin et al. (2024)

6. Conclusions

This study investigated the thermally-induced alterations in the mechanical and elastic parameters of a few dolerite samples from an underground sill. Based on the findings, the following conclusions can be drawn:

(1) The UCS of dolerite exhibited a dual-stage response to thermal treatment, with an initial increase of 15.4% at 250 °C, attributed to drying effects and inherent strengthening of the rock. Beyond 250 °C, UCS progressively decreased due to the initiation and propagation of microcracks, with a significant reduction observed above 450 °C.
(2) Crack propagation in dolerite is temperature-dependent, with no significant microcrack development observed at 250 °C. However, intergranular and intragranular fractures formed at 450 °C and intensified at higher temperatures, as revealed by petrographic and SEM analyses. These cracks disrupted the continuity of the rock matrix, resulting in mechanical weakening and reduced ultrasonic wave velocities.
(3) The brittle-ductile transition in dolerite occurs at 450 °C, as evidenced by changes in the stress-strain response, brittleness index, and elastic properties. At temperatures below 450 °C, dolerite exhibits brittle failure, characterized by abrupt stress drops post-peak. Above this threshold, ductile deformation dominates, with sustained strain in the plastic region before failure.
(4) Static Young's modulus increased up to 250 °C and then decreased from 450 °C to 750 °C, as a result of the formation of intergranular and intragranular microcracks due to thermal stress. Finally, static Poisson's ratio did not change with a robust pattern versus temperature, which confirms a complex deformation behaviour that samples have undergone as a result of exposure to heat.
(5) Finally, the threshold temperature and brittle-ductile transition stage of the dolerite samples should provide critical support for a better implementation of underground UCG projects in the area.

CRediT authorship contribution statement

Chinmay Sethi: Writing – original draft, Validation, Formal analysis, Data curation, Conceptualization. **Bodhisatwa Hazra:** Writing – review & editing, Visualization, Validation, Supervision, Project administration, Methodology, Investigation. **Ali Soleimani:** Visualization, Data curation, Conceptualization. **Mehdi Ostadhassan:** Writing – review & editing, Visualization, Validation, Supervision, Resources, Project administration, Methodology, Investigation, Funding acquisition. **Soumyajit Mukherjee:** Writing – review & editing, Validation. **Dripta Dutta:** Validation, Formal analysis. **Jai Krishna Pandey:** Formal analysis, Data curation.

Declaration of competing interest

The authors declare that they have no known competing financial interests or personal relationships that could have appeared to influence the work reported in this paper.

Acknowledgments

The Director CSIR-CIMFR is thankfully acknowledged for giving permission to conduct this work at CSIR-CIMFR. The authors would like to express gratitude to the editor for giving us another opportunity to revise this paper and submit an improved version. Additionally, our sincere appreciation is extended to the anonymous reviewers who meticulously read this paper and provided us with constructive comments, which significantly enhanced the technical aspects of this manuscript.

References

ASTM D4543, 2010. Standard practices for preparing rock core as cylindrical test spec-imens and verifying conformance to dimensional and shape Tolerances1. Am. Soc. Test Mater.
Barham, W.S., Rabab'ah, S.R., Aldeeky, H.H., Al Hattamleh, O.H., 2020. Mechanical and physical based artifi-cial neural network models for the prediction of the unconfined compressive strength of rock. Geotech. Geol. Eng. 38 (5), 4779–4792.
Blake, O.O., Faulkner, D.R., Tatham, D.J., 2019. The role of fractures, effective pressure and loading on the difference between the static and dynamic Poisson's ratio and Young's modulus of westerly granite. Int. J. Rock Mech. Min. Sci. 116, 87–98.
Brace, W.F., Silver, E., Hadley, K., Goetze, C., 1972. Cracks and pores: a closer look. Science 178 (4057), 162–164.
Chau, K.T., Wong, R.H.C., 1996. Uniaxial compressive strength and point load strength of rocks. In: Int. J. Rock Mech. Min. Sci. Geomech. Abstr., 33. Pergamon, pp. 183–188. No. 2.
Chen, Y.L., Wang, S.R., Ni, J., Azzam, R., Fernandez-Steeger, T.M., 2017. An experimental study of the mechanical properties of granite after high temperature exposure based on mineral characteristics. Eng. Geol. 220, 234–242.
Dwivedi, R.D., Goel, R.K., Prasad, V.V.R., Sinha, A., 2008. Thermo-mechanical properties of Indian and other granites. Int. J. Rock Mech. Min. Sci. 45 (3), 303–315.
Evans, B., Fredrich, J.T., Wong, T.F., 1990. The brittle-ductile transition in rocks: recent experimental and the-oretical progress. The brittle-ductile transition in rocks 56, 1–20.
Gautam, P.K., Verma, A.K., Jha, M.K., Sharma, P., Singh, T.N., 2018. Effect of high temperature on physical and mechanical properties of Jalore granite. J. Appl. Geophys. 159, 460–474.
Hu, J., Sun, Q., Pan, X., 2018. Variation of mechanical properties of granite after high-temperature treatment. Arabian J. Geosci. 11 (2), 1–8.
Huang, Y.H., Yang, S.Q., Tian, W.L., Zhao, J., Ma, D., Zhang, C.S., 2017. Physical and mechanical behaviour of granite containing pre-existing holes after high temperature treatment. Arch. Civ. Mech. Eng. 17 (4), 912–925.
Jena, S.K., Manoj, P., Kuldip, P., 2016. Analysis of strata controll monitoring in rground coal mine for apprehension of strata movement. In: Recent Advances in Rock Engineering (RARE 2016). Atlantis Press, pp. 505–511.
Jiang, Y., Chen, B., Teng, L., Wang, Y., Xiong, F., 2024. Surface subsidence modelling induced by formation of cavities in underground coal gasification. Appl. Sci. 14 (13), 5733.
Jin, Y., He, C., Yao, C., Sun, Z., Wang, J., Zhang, X., Yang, J., Jiang, Q., Zhou, C., 2024. Experimental and numerical simulation study on the evolution of mechanical properties of granite after thermal treatment. Comput. Geotech. 172, 106464.
Kang, H.P., Zhang, X., Si, L.P., Wu, Y., Gao, F., 2010. In-situ stress measurements and stress distribution characteristics in underground coal mines in China. Eng. Geol. 116 (3–4), 333–345.
Klootwijk, C.T., 1974. Palaeomagnetic results on a doleritic sill of deccan trap age in the Sonhat coal basin, India. Tectonophysics 22 (3–4), 335–353.
Laouafa, F., Farret, R., Vidal-Gilbert, S., Kazmierczak, J.B., 2016. Overview and modeling of mechanical and thermomechanical impact of underground coal gasification exploitation. Mitig. Adapt. Strategies Glob. Change 21, 547–576.
Li, X., Wu, Y., Li, Q., Yin, T., Huang, L., 2022. Quantification of thermal damage and dynamic tensile behaviors of hard rock under microwave irradiation: an experimental investigation. Bull. Eng. Geol. Environ. 81 (11), 461.
Liu, S., Xu, J., 2015. An experimental study on the physico-mechanical properties of two post-high-temperature rocks. Eng. Geol. 185, 63–70.
Mahanta, B., Ranjith, P.G., Vishal, V., Singh, T.N., 2020. Temperature-induced deformational responses and mi-crostructural alteration of sandstone. J. Pet. Sci. Eng. 192, 107239.
Malkowski, P., Ostrowski, L., 2017. The methodology for the Young modulus derivation for rocks and its value. In: ISRM EUROCK. ISRM (pp. ISRM-EUROCK).
Ozguven, A., Ozcelik, Y., 2014. Effects of high temperature on physico-mechanical properties of Turkish natu-ral building stones. Eng. Geol. 183, 127–136.
Paul, S., Chattopadhyaya, S., Raina, A.K., Sharma, S., Li, C., Zhang, Y., Kumar, A., Tag-Eldin, E., 2022. A review on the impact of high-temperature treatment on the physico-mechanical, dynamic, and thermal properties of granite. Sustainability 14 (22), 14839.
Qin, Y., Tian, H., Xu, N.X., Chen, Y., 2020. Physical and mechanical properties of granite after high-temperature treatment. Rock Mech. Rock Eng. 53, 305–322.
Ringdalen, E., 2015. Changes in quartz during heating and the possible effects on Si production. Jom 67, 484–492.
Shao, S., Ranjith, P.G., Wasantha, P.L.P., Chen, B.K., 2015. Experimental and numerical studies on the me-chanical behaviour of Australian strathbogie granite at high temperatures: an application to geothermal energy. Geothermics 54, 96–108.

Sharma, R.V., Choudhary, A.K.S., Adak, A.K., Maity, S., 2023. An investigation on demineralization induced modifications in the macromolecular structure and its influence on the thermal behaviour of coking and non-coking coal. J. Mol. Struct. 1274, 134520.
Shojaei, A., Taleghani, A.D., Li, G., 2014. A continuum damage failure model for hydraulic fracturing of porous rocks. Int. J. Plast. 59, 199–212.
Sirdesai, N.N., Singh, T.N., Gamage, R.P., 2017. Thermal alterations in the poro-mechanical characteristic of an Indian sandstone–a comparative study. Eng. Geol. 226, 208–220.
Sun, Q., Zhang, W., Xue, L., Zhang, Z., Su, T., 2015. Thermal damage pattern and thresholds of granite. Environ. Earth Sci. 74 (3), 2341–2349.
Sun, Q., Zhang, W., Zhu, Y., Huang, Z., 2019. Effect of high temperatures on the thermal properties of granite. Rock Mech. Rock Eng. 52 (8), 2691–2699.
Tian, H., Kempka, T., Yu, S., Ziegler, M., 2016. Mechanical properties of sandstones exposed to high temperature. Rock Mech. Rock Eng. 49, 321–327.
Tian, H., Mei, G., Jiang, G.S., Qin, Y., 2017. High-temperature influence on mechanical properties of diorite. Rock Mech. Rock Eng. 50 (6), 1661–1666.
Vagnon, F., Colombero, C., Colombo, F., Comina, C., Ferrero, A.M., Mandrone, G., Vinciguerra, S.C., 2019. Effects of thermal treatment on physical and mechanical properties of Valdieri Marble-NW Italy. Int. J. Rock Mech. Min. Sci. 116, 75–86.
Wang, F., Frühwirt, T., Konietzky, H., 2020. Influence of repeated heating on physical-mechanical properties and damage evolution of granite. Int. J. Rock Mech. Min. Sci. 136, 104514.
Watanabe, T., Tomioka, A., Yoshida, K., 2024. The closure of microcracks under pressure: inference from elastic wave velocity and electrical conductivity in granitic rocks. Earth Planets Space 76 (1), 153.
Xu, X., Kang, Z., Ji, M., Ge, W., Chen, J., 2009. Research of microcosmic mechanism of brittle-plastic transition for granite under high temperature. Proc. Earth Planet. Sci. 1 (1), 432–437.
Yang, S.Q., Li, Y., Ma, G.W., Sun, B.W., Yang, J., Xu, J., Dai, Y.H., 2023. Experiment and numerical simulation study of dynamic mechanical behavior of granite specimen after high temperature treatment. Comput. Geotech. 154, 105111.
Yin, T.B., Shu, R.H., Li, X.B., Pin, W.A.N.G., Liu, X.L., 2016. Comparison of mechanical properties in high temperature and thermal treatment granite. Trans. Nonferrous Metals Soc. China 26 (7), 1926–1937.
Yin, S., Mei, H., Xu, X., 2023. Experimental study on dynamic and static rock mechanical properties of tight sandstone gas reservoir. Chem. Technol. Fuels Oils 59 (3), 561–568.
Zhang, W., Sun, Q., Hao, S., Geng, J., Lv, C., 2016. Experimental study on the variation of physical and mechanical properties of rock after high temperature treatment. Appl. Therm. Eng. 98, 1297–1304.
Zhang, F., Zhao, J., Hu, D., Skoczylas, F., Shao, J., 2018. Laboratory investigation on physical and mechanical properties of granite after heating and water-cooling treatment. Rock Mech. Rock Eng. 51, 677–694.
Zhang, Y., Zhang, F., Yang, K., Cai, Z., 2022. Effects of real-time high temperature and loading rate on deformation and strength behavior of granite. Geofluids 2022 (1), 9426378.
Zhu, Z., Tian, H., Mei, G., Jiang, G., Dou, B., Xiao, P., 2021. Experimental investigation on mechanical behaviors of Nanan granite after thermal treatment under conventional triaxial compression. Environ. Earth Sci. 80, 1–14.

Dr. Chinmay Sethi holds graduate and Postgraduate degrees from Central University of Karnataka (India). He recently defended his Ph.D. thesis for his work on the organo-petrographic characteristics, source rock potential, and palaeo-depositional settings of shales of contrasting thermal maturities. Dr. Sethi's research interests include organic petrology, source rock geochemistry, geomechanics, and CO_2 storage. He has published multiple research articles in high-impact journals. His work has been presented at national and international conferences, where he has also received recognition, including a Best Paper Award at ICGEID 2024 hosted by IIT-Patna.